Chalcogenide Letters Vol. 22, No. 12, December 2025, p. 1055-1066

Laser-Ablated CdS and Ag_2O Nanomaterials for High-Sensitivity Photodetectors

Hameed H. Ahmed[1], Thaer A. Mezher[2,*] and Marwan R. Rashid[3]

[1]Department of Mechanics Engineering, College of Al-Shirgat Engineering, Tikrit University, Tikrit, 34001, Iraq
[2]Directorate General of Education in Diyala, Baqubah, 32001, Iraq
[3]Department of Physics, College of Education for Pure Sciences, University of Diyala, Baqubah, 32001, Iraq
*Corresponding Author: Thaer A. Mezher. Email: thier.thier81@gmail.com

Received: 28 September 2025; Accepted: 10 December 2025

ABSTRACT: Laser ablation in liquids (LAL), a hygienic and effective method for creating high-purity nanomaterials, was used in this study to create cadmium sulfide (CdS) and silver oxide (Ag_2O) nanoparticles. The sputtering process was used to deposit the produced nanomaterials on porous silicon (PSi) substrates, and a number of assays were used to examine the samples' structural, optical, and electrical characteristics. The CdS sample had a hexagonal crystal structure, according to X-ray diffraction (XRD) data, whereas the AgO sample had a cubic structure. The diameters of the nanoparticles in the two samples ranged from 22.64 nm for CdS to 32.69 nm for AgO. The CdS sample had almost normal spherical particles, according to scanning electron microscopy (SEM) pictures, whereas the AgO sample had cluster formations. The CdS sample's surface roughness was 4.78 nm, while the AgO sample's was 9.14 nm, according to atomic energy microscopy (AFM) photographs. The optical energy gap (Eg) for the CdS and AgO samples, as determined by UV-Vis spectroscopic tests, was 6.4 eV and 5.52 eV, respectively. This indicates a distinct change in characteristics brought about by nanoscale size and quantum effects. Analysis was done on optical constants like the dielectric constant, optical conductivity, extinction coefficient, and refractive index. Additionally, the Ag/AgO/CdS/PSi thin film's photovoltaic characteristics were examined. With a particular sensitivity of ($D^* = 1.2 \times 1011$ Jones) and a quantum efficiency of ($Q \approx 89\%$), the composite demonstrated a wide spectrum response from 350 to 1050 nm. These findings demonstrate that the Ag/AgO/CdS/PSi thin film has exceptional qualities that make it a promising option for photovoltaic and photodetector applications, especially in the visible and near-infrared spectrum.

KEYWORDS: Laser ablation in liquids; nanoparticles; CdS; Ag_2O; photodetectors; thin films; quantum efficiency; spectral responsivity

1 Introduction

Nanostructured semiconductor materials have garnered significant attention in recent years due to their promising applications in optoelectronic devices, particularly in photodetectors, solar cells, and sensors. Among these materials, cadmium sulfide (CdS) and silver oxide (Ag_2O) stand out due to their suitable band gaps, chemical stability, and tunable optical properties, making them ideal candidates for light-sensitive applications [1,2].

Laser Ablation in Liquid (LAL), one of the newer physical synthesis methods for creating high-purity nanomaterials, provides a "green" and surfactant-free way to create nanoparticles with precise size and shape. This method creates colloidal nanoparticles free of chemical contamination by directing intense laser pulses onto a solid target immersed in a liquid media [3,4]. By varying variables including laser wavelength, pulse energy, ablation time, and the type of ambient liquid, the resultant nanostructures' physicochemical characteristics can be customized [5]. There are still issues with preserving structural purity and extending the spectral response range, particularly when employing traditional preparation techniques that could leave chemical residues that impair performance, even after a large number of prior studies addressing the use of nanomaterials to improve

https://doi.org/10.15251/CL.2025.2212.1055

photodetector performance. Therefore, the purpose of this study is to use laser ablation in a deionized aqueous medium to create pure CdS and AgO nanoparticles. We examine their electrical, optical, and structural characteristics and assess how well they work to create a highly sensitive Ag/Ag_2O/CdS/Si photodetector, offering a practical and sustainable substitute that can be used in upcoming photonic applications.

In the present study, CdS and Ag_2O nanoparticles were synthesized via the LAL method in deionized water, and subsequently deposited as thin films on n-type silicon substrates using the drop casting technique. This approach allows for the formation of uniform and adherent thin films suitable for device fabrication. The prepared films were thoroughly characterized using structural and optical analysis techniques to evaluate their potential in photodetector applications. Specifically, quantum efficiency and spectral responsivity measurements were conducted to assess the photo detection performance of the films.

2 Experimental Part

2.1 Substrate Preparation

Glass slides and n-type porous silicon (PSi) wafers were used as substrates. Glass substrates (1.5 × 1.5 cm^2) were cleaned in a dilute detergent solution at 70–100°C using an ultrasonic bath, followed by rinsing with hot deionized and distilled water, and stored in methanol. Prior to deposition, they were dried using hot air. Silicon wafers were ultrasonically cleaned in ethanol, then immersed in 10% HF solution for 5 min to remove the native oxide layer. PSi layers of varying thicknesses were fabricated using electrochemical (EC) and photo electrochemical (PEC) etching techniques.

2.2 Synthesis of Ag_2O and CdS Nanoparticles

Silver (Ag_2O) and cadmium sulfide (CdS) nanoparticles were synthesized by pulsed laser ablation in liquid (PLAL) using a Nd:YAG laser (λ = 1064 nm, 7 ns, 5 Hz). Compressed Ag and CdS targets were irradiated in 5 mL of deionized water at (400) pulses with energy (600) mJ. This resulted in stable colloidal nanoparticle suspensions.

2.3 Thin Film Deposition

Thin films were deposited on PSi substrates via the drop-casting technique (Fig 1) by applying a controlled volume of the nanoparticle solution and allowing it to dry at room temperature, forming the photodetector's active layer.

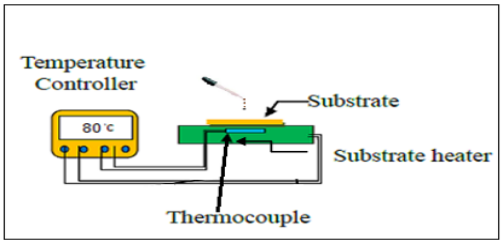

Figure 1: Schematic diagram drop casting method experimental set up.

2.4 Structural and Morphological Characterization

To examine the crystallinity and phase structure of the produced nanomaterials, X-ray diffraction (XRD) was utilized. Grain distribution, surface roughness, and surface morphology were examined using atomic force microscopy (AFM) and scanning electron microscopy (SEM). The optical characteristics were further

investigated using ultraviolet–visible (UV–Vis) spectroscopy, which allowed for the determination of the transmittance, absorbance, and optical bandgap (Eg). To fully comprehend how light interacts with the nanostructured CdS and AgO materials, additional important optical constants were computed using the UV-Vis data. These included the refractive index (n), extinction coefficient (k), real (εr) and imaginary (εi) components of the dielectric constant, and the optical conductivity (σ_{opt}).

2.5 Photodetector Performance Evaluation

Spectral responsivity (R_λ) was measured using a UIR-210A double-beam spectrophotometer (200–1000 nm), and photocurrent was recorded with a Fluke 8010 DMM. Specific detectivity (D) and quantum efficiency (Q) were calculated from standard equations based on the measured responsivity and noise characteristics.

3 Results

3.1 X-ray Diffraction Analysis

Fig. 2 shows the XRD patterns of CdS and Ag_2O nanoparticles synthesized via the PLAL technique. The sharp and intense peaks of CdS indicate a high degree of crystallinity, which is essential for reducing defect-related recombination and improving carrier mobility—key factors in enhancing photodetector efficiency. In contrast, the broad peaks of Ag_2O reflect its nanocrystalline nature and small crystallite size, which increases surface area and enhances interaction with light, beneficial for broadband UV-visible detection. The structural integrity and distinct phases (CdS: hexagonal, Ag_2O: cubic) as confirmed by JCPDS standards (No. 41-1049 and 41-1104) suggest the potential of each material for tunable and hybrid photodetector architectures, where crystalline CdS ensures charge transport and Ag_2O contributes to enhanced light absorption and sensitivity [6].

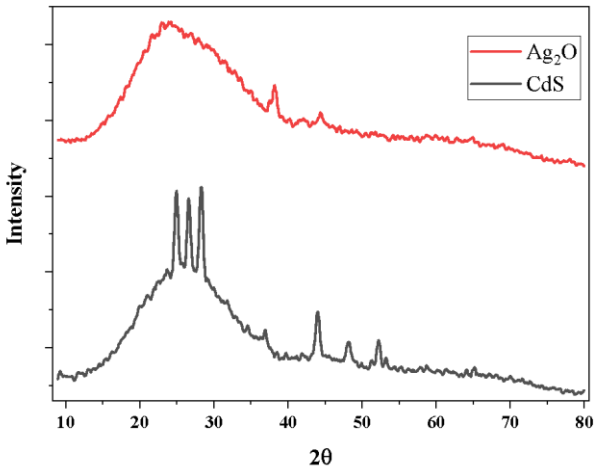

Figure 2: The X-ray diffraction of silver oxide and cadmium sulfide ablated by laser.

3.2 FESEM Analysis

The SEM images in Fig. 3, reveal that the CdS and Ag_2O nanoparticles prepared via PLA exhibit predominantly spherical morphology, with particle sizes ranging between 21–47 nm. CdS particles appear well-distributed, while Ag_2O particles tend to aggregate into clusters, possibly due to higher surface energy. they enhance the surface-to volume ratio, facilitate efficient light absorption, and promote carrier separation and transport, which are essential for achieving high sensitivity and fast response in optoelectronic devices [7].

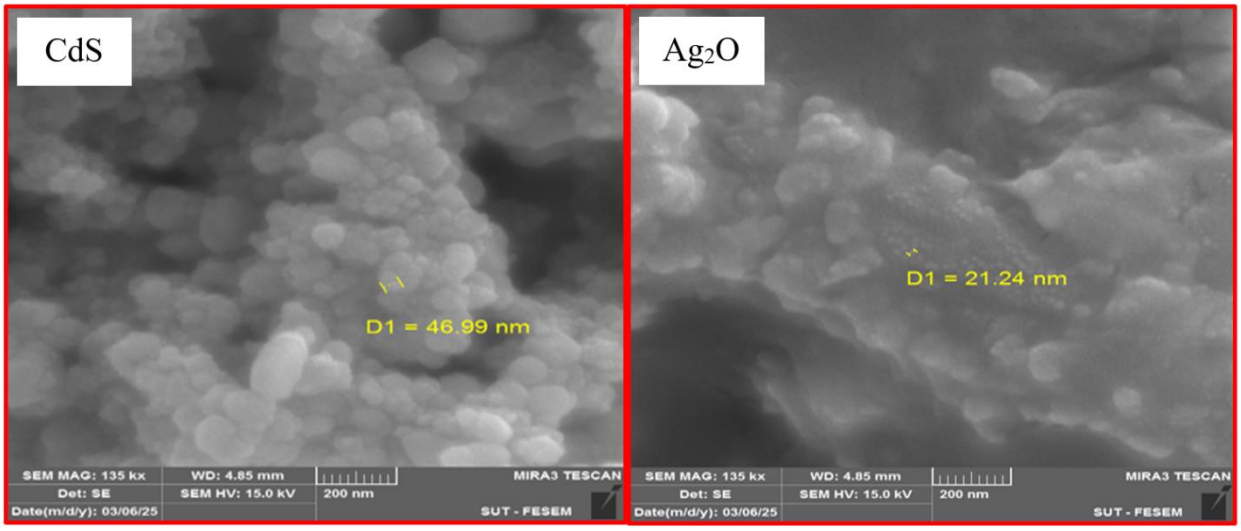

Figure 3: Scanning electron microscope images.

3.3 AFM Analysis

AFM pictures of CdS and AgO nanoparticles made by laser ablation in liquid are shown in Fig. 4, where the surface roughness and particle height distribution clearly differ. The smoother surface and lower average height of CdS nanoparticles suggest more uniform crystallite development, which is advantageous for improving charge transfer and lowering surface recombination in photodetectors. AgO, on the other hand, exhibits greater surface roughness and greater height fluctuations, most likely as a result of metallic clustering and aggregation. These characteristics might improve light scattering and surface reactivity, which may improve the interaction between light and matter in photodetection systems. These distinct morphological features support the complementary roles of CdS and Ag_2O in designing hybrid or composite photodetectors with optimized performance [8].

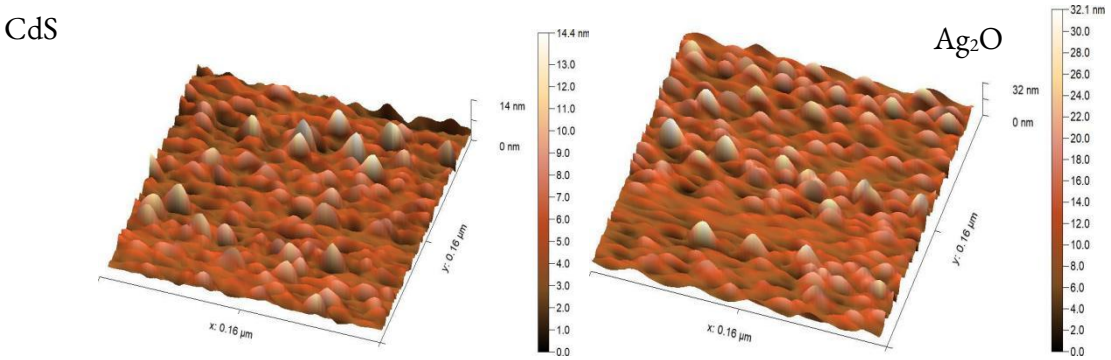

Figure 4: AFM analysis.

3.4 Optical Properties

Fig. 5 right shows the optical absorbance spectra of CdS nanoparticles synthesized by laser ablation in deionized water. The spectrum reveals a pronounced absorbance in the ultraviolet (UV) region (below ~400 nm), which rapidly decreases and stabilizes at a low level across the visible and near-infrared (NIR) ranges (500–1100 nm). This optical behavior indicates that CdS nanoparticles possess a wide bandgap that facilitates strong absorption of high-energy photons in the UV region, this agreement with [9]. where the low absorbance in the

visible/NIR regions minimizes noise and enhances selectivity, making CdS a promising candidate for UV-selective photodetectors. Additionally, the sharp absorbance edge suggests good crystallinity and well-defined optical transitions, which contribute to efficient photo generation of charge carriers when exposed to UV light. Fig. 5 left presents the absorbance spectrum of Ag_2O nanoparticles, showing strong optical absorption in the deep UV and visible regions, with a prominent peak around 400 nm, and gradually decreasing absorbance toward the near-infrared (NIR) region. The absorbance exceeds 0.6 below 330 nm, indicating significant photon absorption at high energies, while the absorbance approaches zero beyond 700 nm, reflecting high transparency in the NIR range. The UV-visible absorption enhances photo response sensitivity to high-energy photons, while the NIR transparency reduces background interference and allows for integration with other absorbing layers in multilayer or tandem detector systems. Furthermore, the dip in the 550–650 nm range suggests defect-level transitions, which can be engineered to tailor the material's spectral selectivity in optoelectronic applications [10].

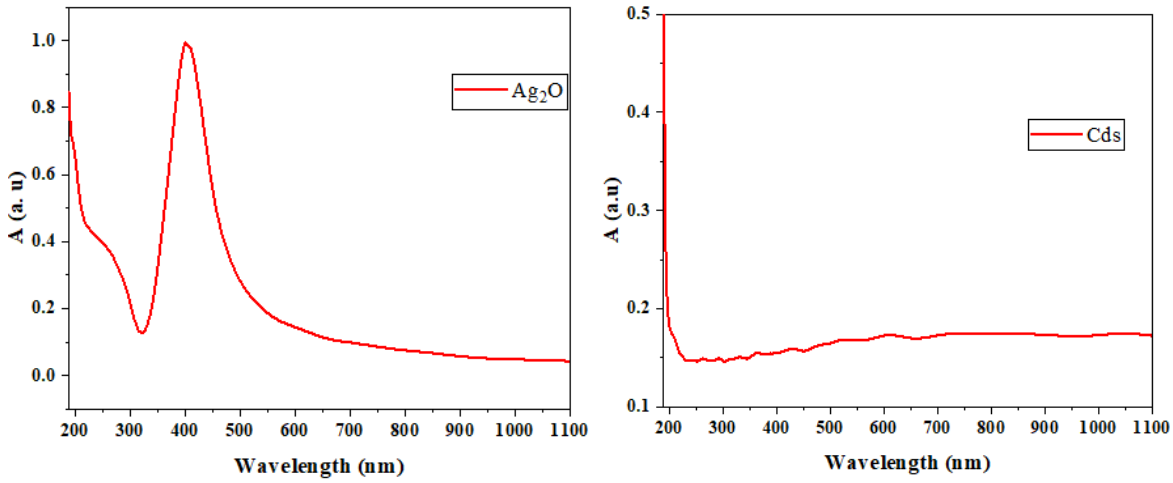

Figure 5: The absorbance (A) of the prepared CdS and Ag_2O particles.

The Tauc plot of $(\alpha h\nu)^2$ vs photon energy $h\nu$ for CdS nanoparticles produced by laser ablation in deionized water is shown in Fig. 6 right. The material's direct band gap nature is confirmed by the observed linear region. From the extrapolation of the linear portion, the optical band gap (Eg) was estimated to be 6.4 eV, which is significantly higher than the bulk CdS value (~2.42 eV). The quantum confinement effect resulting from the smaller particle size, a common consequence of the laser ablation synthesis process, is responsible for this considerable increase [11]. Where the large band gap, enables the material to absorb and respond to high-energy UV photons while remaining transparent to visible and infrared radiation. Furthermore, the direct nature of the band gap ensures efficient generation and separation of photo generated carriers, which improves the responsivity and speed. Fig. 6 left displays the Tauc plot for Ag_2O nanoparticles, showing a direct optical band gap of approximately 5.52 eV, corresponding to strong absorption in the deep UV region. Additionally, a distinct absorption feature appears around 2.9 eV (≈430 nm), attributed to defect-induced transitions or Surface Plasmon Resonance (SPR) effects from embedded silver nanoparticles within the oxide matrix. The wide band gap enables high selectivity toward high-energy UV photons, while the visible-region absorption peak—influenced by plasmonic effects—enhances light-matter interaction and improves photocurrent

generation in the visible range. These characteristics support the use of Ag_2O in multi-band and hybrid photodetectors, combining high sensitivity with spectral tunability [12].

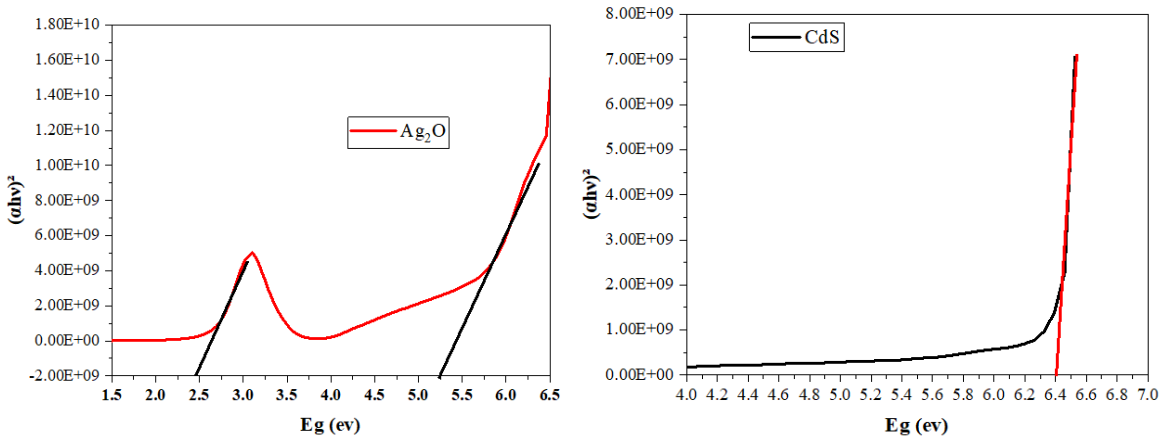

Figure 6: The Energy Gap (Eg) of the prepared CdS and Ag_2O particles.

Fig. 7 right presents the variation of both the extinction coefficient (k) and the refractive index (n) as functions of wavelength for CdS nanoparticles. The extinction coefficient exhibits a strong rise in the ultraviolet region, followed by a sharp decline beyond the absorption edge. This trend reflects the high absorption of UV photons and a significant reduction in absorption at longer wavelengths. The persistence of a non-zero *k* even beyond the band edge can be attributed to light scattering and absorption at grain boundaries. Simultaneously, the refractive index shows two well-defined maxima and minima across the measured spectrum, which can be attributed to interference effects and structural in homogeneities in the CdS nanoparticles. These oscillations indicate strong interaction of the incident light with the material, supporting its potential for efficient light manipulation and guiding. The combination of high UV absorption (high k) and variable refractive index (high n) strongly benefits photodetector applications, especially in the UV range [13]. The strong absorption ensures efficient photon–carrier conversion, while the modulation in refractive index facilitates enhanced light–matter interaction, critical for improving device responsivity and optical gain. Fig. 7 left shows the refractive index (n) and extinction coefficient (k) of Ag_2O nanoparticles as functions of wavelength. Both parameters increase and reach their respective peaks at ≈300 nm (n) and ≈450 nm (k), indicating strong photon–material interaction and optical absorption in the UV to visible range. Beyond 500 nm, both values decline steadily, confirming the material's increasing transparency toward the near-infrared region. At 700 nm, values of n ≈ 2.51 and k ≈ 0.012 agree with literature reports [14]. Where a high refractive index and extinction coefficient in the UV/visible region support efficient light absorption and confinement, while their reduction in the NIR ensures low-loss transmission. Such characteristics are ideal for achieving broadband sensitivity, spectral selectivity, and improved photocurrent generation.

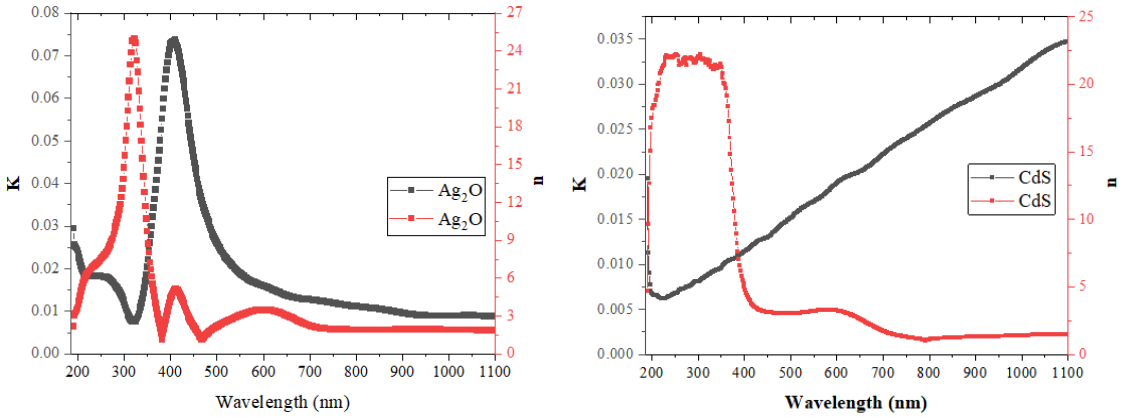

Figure 7: The extinction coefficient and refractive index of the prepared particles.

Fig. 8 right illustrates the variation of optical conductivity (σopt) of CdS nanoparticles as a function of wavelength. A pronounced enhancement in conductivity is observed at shorter wavelengths, particularly in the UV region (200–400 nm). This behavior is directly correlated with the high absorbance of CdS in this spectral range, as previously shown in Fig. 5. The increased absorbance leads to a higher generation rate of charge carriers (electrons and holes), resulting in improved optical conductivity. High optical conductivity translates to better carrier mobility and reduced recombination losses, enhancing the photo response and charge extraction efficiency. These properties are particularly advantageous in UV photodetectors, where fast and efficient carrier transport is essential for achieving high-speed detection and strong signal amplification [15]. Where both strong absorption and efficient electrical conduction are required for optimal performance. Fig. 8 left illustrates the variation of optical photoconductivity of Ag_2O nanoparticles as a function of wavelength. The photoconductivity increases sharply up to 500 nm, indicating efficient generation of photo-induced charge carriers in the UV-visible region, likely due to a high density of electronic states within the band gap. Beyond this point, the conductivity decreases gradually with increasing wavelength, reflecting a reduction in carrier generation as photon energy diminishes agree with the findings reported by [16]. This wavelength-dependent behavior is a strong indicator of photo response sensitivity in the visible range. The significant photoconductivity in the 300–500 nm region enhances charge transport and photocurrent production, essential for achieving high-efficiency optoelectronic performance.

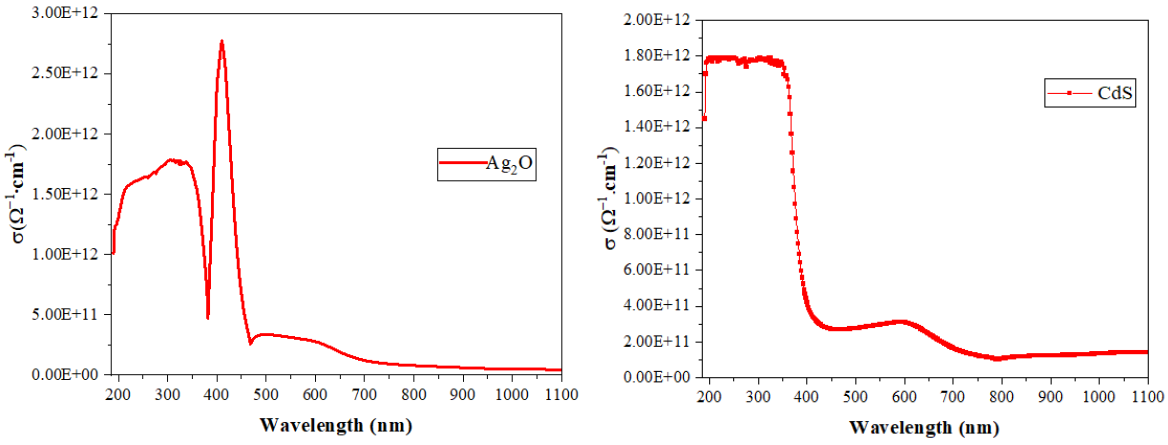

Figure 8: show the optical conductivity of the prepared particles.

Fig. 9 right shows the variations in the real (εr) and imaginary (εi) parts of the dielectric constant of CdS nanoparticles as a function of wavelength. A prominent peak in both εr and εi appears near 370 nm, corresponding to high absorption of UV photons due to direct inter band electronic transitions. These peaks reflect the material's strong interaction with incident electromagnetic waves in the UV region, indicative of high optical polarization and carrier excitation activity. The subsequent decrease in both εr and εi at longer wavelengths signifies a lower probability of photon-induced electronic transitions as photon energy decreases, indicating that the material becomes increasingly transparent in the visible and near-infrared regions. The peak in the real part (εr) suggests strong photon-induced polarization, enhancing light–matter interaction, while the imaginary part (εi) is directly linked to energy loss mechanisms primarily absorption which confirms efficient photon absorption in the UV range [17]. Together, these properties reinforce the potential of CdS nanoparticles for high-sensitivity and fast-response UV photodetectors, where rapid electronic polarization and strong absorption are essential for converting incoming light into electrical signals effectively. Fig. 9 left shows the dependence of the real (εr) and imaginary (εi) parts of the dielectric constant of Ag_2O nanoparticles on wavelength. The real part (εr) decreases progressively with increasing wavelength, indicating reduced polarization capability and energy retention at lower photon energies. This reflects the degree of photon deceleration and gives insight into energy loss mechanisms within the material an important factor in light material interaction. The imaginary part (εi) follows a similar profile to the extinction coefficient K, due to its strong dependence on it, representing energy dissipation or optical absorption losses within the material. The behavior of εi across the spectrum confirms Ag_2O's strong photon absorption capabilities in the UV-visible region. Such dielectric behavior is vital for photodetector applications, as it ensures enhanced optical response, efficient carrier excitation, and controlled loss mechanisms, all contributing to the selectivity and sensitivity of Ag_2O-based photodetectors [17].

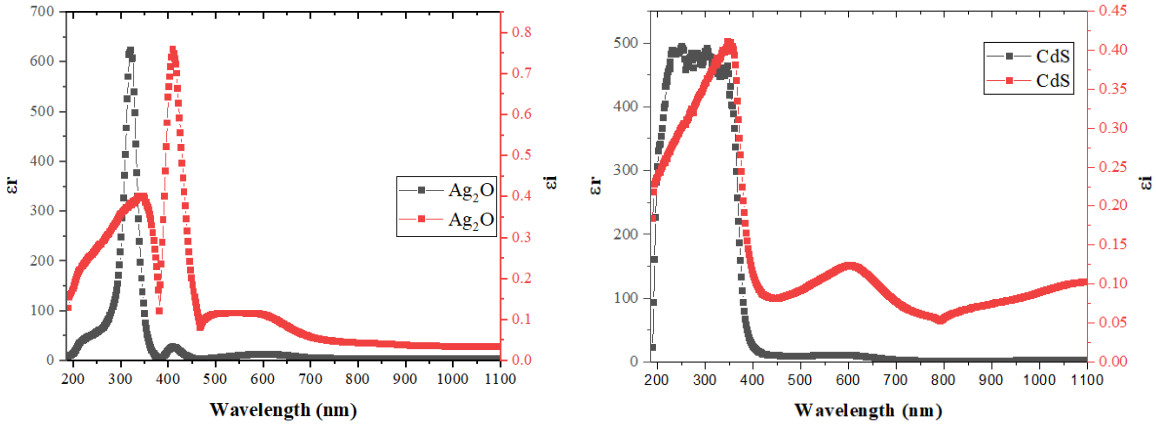

Figure 9: The variations in the real (εr) and imaginary (εi) parts of the dielectric constant of CdS and Ag_2O particles.

3.5 Specific Responsivity (Rλ)

Fig. 10 shwos the responsivity (I/P) versus wavelength for Ag/CdS/Si, Ag/Ag_2O/Si, and Ag/Ag_2O/CdS/Si photodetectors. The Ag/CdS/Si sample shows a pronounced peak around 580–600 nm, corresponding to the CdS bandgap (~2.4 eV) and its efficient absorption in the green-yellow region. In contrast, Ag/Ag_2O/Si demonstrates a lower and relatively flat response across the spectrum, due to Ag_2O's limited light absorption and its primary role in charge transport. The Ag/Ag_2O/CdS/Si composite exhibited superior responsivity, with two distinct peaks at 550 nm and ~900 nm, indicating synergistic absorption from CdS in the visible range and silicon in the near-infrared. Overall, the Ag/Ag_2O/CdS/Si structure combines the optical absorption strengths of CdS

and silicon with the electronic advantages provided by oxide silver, resulting in a broad and enhanced spectral response [18].

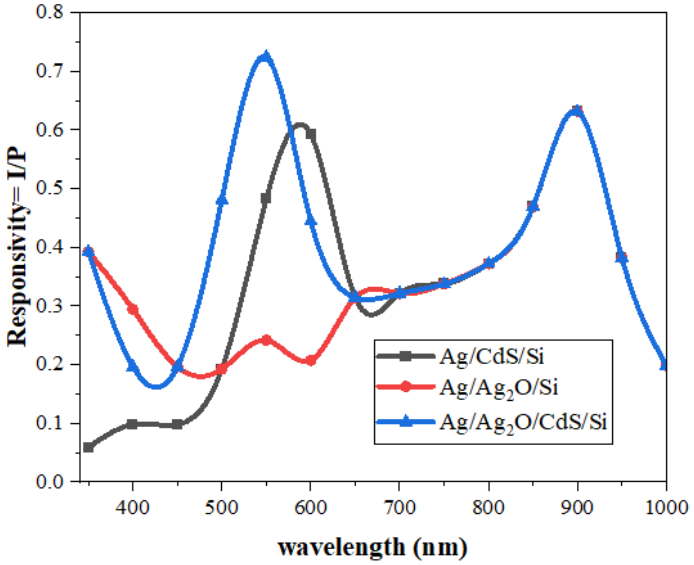

Figure 10: The responsivity for samples.

3.6 Specific Detection (D)*

Fig. 11 shows the detection (D) versus wavelength for three photodetector nanostructures: Ag/CdS/Si, Ag/Ag_2O/Si, and Ag/Ag_2O/CdS/Si. The Ag/Ag2O/CdS/Si sample exhibited the highest detection, with peaks at 550 nm and 900 nm, combining the strengths of CdS for visible light absorption and silicon for near-infrared. The Ag/CdS/Si sample showed a detection peak at 600 nm but performed poorly in the infrared, while Ag/Ag_2O/Si exhibited low overall detection, with a slight improvement at 800 nm due to silicon absorption. The limited effect of Ag_2O on light absorption accounts for its average performance. Overall, Ag/Ag_2O/CdS/Si delivers the best detection efficiency by integrating the optical and electronic advantages of its components, outperforming the other compositions across a broader wavelength range [19].

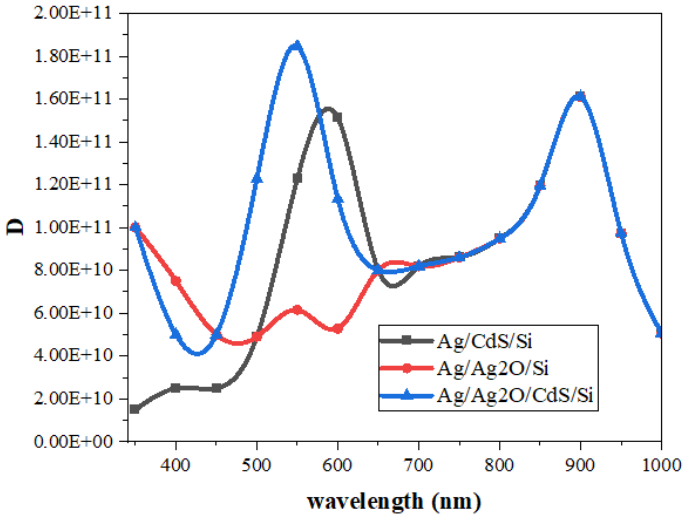

Figure 11: Shows the detection (D) versus wavelength for three photodetector nanostructures.

3.7 Quantum Efficiency

Fig. 12 shows the quantum efficiency (Q) versus wavelength for three nanostructures: Ag/CdS/Si, Ag/Ag_2O/Si, and Ag/Ag_2O/CdS/Si. The Ag/Ag_2O/CdS/Si structure outperforms others, with peaks at 550 nm and 900 nm, due to the complementary roles of CdS (visible absorption), Si (near-infrared absorption), and Ag_2O (enhancing charge separation). Oxide silver enhances absorption through plasmonic effects, boosting Q values, especially in the ternary structure. The Ag/CdS/Si structure shows a peak at 600 nm but declines beyond that due to the absence of Ag_2O, which affects charge separation. The Ag/Ag_2O/Si sample has a stable but lower performance, lacking CdS for efficient visible light absorption. Oxide silver enhances electron transport and absorption in all structures, but the optimized layer arrangement in Ag/Ag_2O/CdS/Si leads to superior performance, making it ideal for broad-spectrum photodetectors and solar cells [20,21].

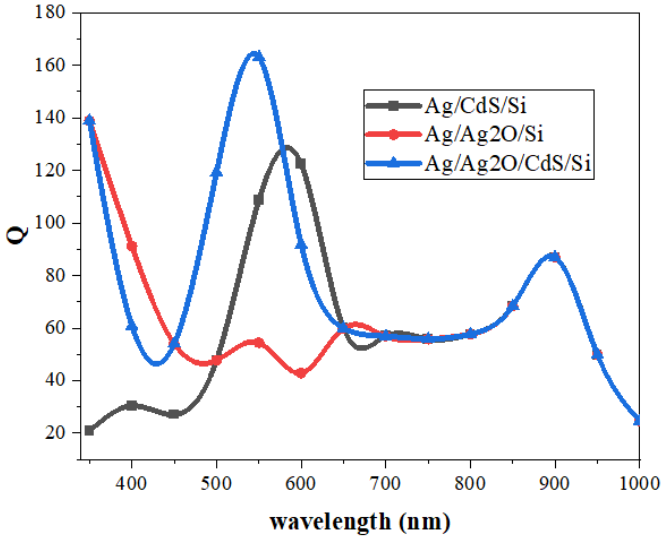

Figure 12: The quantum efficiency (Q) versus wavelength for three nanostructures.

4 Conclusions

The results of this research demonstrated that laser ablation in liquids (LAL) is an effective and environmentally friendly method for preparing nanoparticles from semiconductor materials such as CdS and Ag_2O without the need for chemical additives. XRD examinations revealed that the prepared particles possessed distinct crystalline phases. CdS had a hexagonal structure with an average crystal size of 22.64 nm, while Ag_2O exhibited a cubic structure with an average size of 32.69 nm. SEM and AFM images revealed distinct differences in surface structure. CdS particles had a homogeneous surface and relative smoothness (surface roughness ≈ 4.78 nm), while Ag_2O particles exhibited clustering and higher roughness (≈9.14 nm). FTIR analysis confirmed the successful preparation through the appearance of distinct chemical bonds such as Cd–S and Ag–O. Optically, the UV-Vis spectra showed a clear transition in the energy bandgap due to the quantum effect, with Eg ≈ 6.4 eV for the CdS sample and 5.52 eV for the Ag_2O sample. Using the Ag/Ag_2O/CdS/PSi integrated structure, the prepared samples exhibited a broad spectral response from 350 to 1050 nm, with a quantum efficiency of 89% and a specific sensitivity of 1.2×10^{11} Jones, reflecting a significant improvement in photovoltaic performance. The synergy between the three materials resulted in enhanced light absorption and charge

transport, making this structure highly promising for photodetector and solar cell applications with a broad spectral absorption range.

Acknowledgement: Not applicable.

Funding Statement: The authors received no specific funding for this study

Author Contributions: Each co-author has made unique contributions to the work. The author Hameed H. Ahmed prepared the thin films and contributed to writing the article. Thaer A. Mezher supervised the work and contributed to the analysis of the results. As the author, Marwan R. Rashid wrote the program for photodetector properties. All authors reviewed the results and approved the final version of the manuscript

Availability of Data and Materials: The data that support the findings of this study are available from the corresponding author（Thaer A. Mezher）upon reasonable request

Ethics Approval:Not applicable. This study did not involve human or animal subjects.

Conflicts of Interest: The authors declare no conflicts of interest to report regarding the present study

References

1. Ferrá-González SR, Berman-Mendoza D, García-Gutiérrez R, Castillo SJ, Ramírez-Bon R, Gnade BE, et al. Optical and structural properties of CdS thin films grown by chemical bath deposition doped with Ag by ion exchange. Optik. 2014;125(4):1533–6. http://doi.org/10.1016/j.ijleo.2013.08.035.
2. Mezher TA, Ahmed HH, Khaleel MM. CdO Nanoparticles by chemical method as antimicrobial therapy in order to maintain of healthy cells. J Phys Conf Ser. 2024;2857(1):012015.
3. Karthikeyan N, Thiruramanathan P, Srinivasan R, Sivamurugan R, Sahaya Dennish Babu G. Pulsed laser–produced nanomaterials in liquids for biomedical applications. In: Pulsed laser-induced nanostructures in liquids for energy and environmental applications. Amsterdam, The Netherland: Elsevier; 2024. p. 243–69. http://doi.org/10.1016/b978-0-443-13379-4.00015-8.
4. Ajaj K, Ali AM, Al-Jubbori MA. Characterization and evaluation of the antimicrobial activity of CuO nanoparticles prepared by pulse laser ablation in double-distilled water. Nanosistemi Nanomater Nanotehnologii. 2024;22(1):209–27.
5. Barcikowski S, Compagnini G. Advanced nanoparticle generation and excitation by lasers in liquids. Phys Chem Chem Phys. 2013;15(9):3022–6. http://doi.org/10.1039/c2cp90132c.
6. Soto E, Vaquero F, Mota N, Navarro RM, Fierro JLG. CdS photocatalysts modified with Ag: effect of the solvothermal temperature on the structure and photoactivity for hydrogen production. Catalysts. 2019; 9(2):110. http://doi.org/10.3390/catal9020110.
7. Hu X, Li X, Li G, Ji T, Ai F, Wu J, et al. Recent progress of methods to enhance photovoltaic effect for self-powered heterojunction photodetectors and their applications in inorganic low-dimensional structures. Adv Funct Mater. 2021;31(24):2011284. http://doi.org/10.1002/adfm.202011284.
8. Falcaro P, Ricco R, Yazdi A, Imaz I, Furukawa S, Maspoch D, et al. Application of metal and metal oxide nanoparticles@MOFs. Coord Chem Rev. 2016;307:237–54. http://doi.org/10.1016/j.ccr.2015.08.002.
9. Bharti DB, Bharati AV, Wankhade AV. Synthesis, characterization and optical property investigation of CdS nanoparticles. Luminescence. 2018;33(8):1445–9. http://doi.org/10.1002/bio.3572.
10. Gangopadhyay P. Optical, photoluminescence, and vibrational spectroscopy of metal nanoparticles. In: Semiconductor nanocrystals and metal nanoparticles. Boca Raton, FL, USA: CRC Press; 2016. p. 127–89. http://doi.org/10.1201/9781315374628-5.
11. Amroun MN, Khadraoui M, Miloua R, Kebbab Z, Sahraoui K. Investigation on the structural, optical and electrical properties of mixed SnS_2–CdS thin films. Optik. 2017;131:152–64. http://doi.org/10.1016/j.ijleo.2016.11.005.
12. Din HU, Reshak AH. Structural, elastic, thermal, electronic and optical properties of Ag_2O under pressure. Comput Mater Sci. 2014;83:474–80. http://doi.org/10.1016/j.commatsci.2013.11.021.
13. Mezher TA, Ahmed HH, Dhari AH. Antimicrobial activity of Al_2O_3 nanoparticles prepared by simple chemical method. Iraqi J Appl Phys. 2024;20(3B):651–4.

14. Fakhri MA, BaderBA, Khalid FG, Mohammed AZ, Shgathi AA. Optical investigations and optical constants of nano silver oxide prepared by PLD method. Sci Int. 2018;30:33–6.
15. Abid HA, Al-Rashid SNT. Study of the effect of nanoparticle size on the dielectric constant and concentration of charge carriers of Si and CdS materials. Chalcogenide Lett. 2020; 17(12):623–9. http://doi.org/10.15251/cl.2020.1712.623.
16. Ali ZS, Dahham NA. Photoresponse characteristics of Ppy/Ag_2O nanocomposites synthesized by hydrothermal method. Iraqi J Appl Phys. 2024;20(2B):375–80.
17. Karim HJA, Al-Azzawi BF, Hammadi ME, Mohammed GH. Influence of Ag_2O doping on structural and optical properties of thin Bi_2O_3 films prepared by pulse laser deposition technique. J Opt. 2025; 54(5):3469–78. http://doi.org/10.1007/s12596-024-01944-5.
18. Fakhri MA, Numan NH, Mohammed QQ, Abdulla MS, Hassan OS, Abduljabar SA, et al. Responsivity and response time of nano silver oxide on silicon heterojunction detector. Work. 2018;16:18.
19. Park T, Park S, Park JH, Min JY, Jung Y, Kyoung S, et al. Temperature-dependent self-powered solar-blind photodetector based on Ag_2O/β-Ga_2O_3 heterojunction. Nanomaterials. 2022; 12(17):2983. http://doi.org/10.3390/nano12172983.
20. Yahya AM, Hassan AI, Salim ET, Addie AJ. Hybrid nanocomposites for enhanced photodetection: synthesis and application of Ag_2O@Graphene/Si heterojunctions. J Alloys Compd. 2024; 1001:175133. http://doi.org/10.1016/j.jallcom.2024.175133.
21. Hanfoosh SM, Aadim KA, Razeg KH. Using the plasma jet method to create zinc nanoparticles and study their structural and optical properties as an NH_3 gas sensor. Int J Nanosci. 2024; 23(6):2350072. http://doi.org/10.1142/s0219581x23500722.